

## BEHAVIOR OF CFDST COLUMNS WITH OCTAGON AND POLYGON STEEL SECTIONS

Ebrahim Farajpourbonab<sup>1\*</sup> and Amin Rafieioskoei<sup>2</sup>

<sup>1</sup>Department of Civil Engineering, S.P Pune University, India

<sup>2</sup>Department of Geography and Urban Planning, Islamic Azad University, Tabriz Branch

Received 09 July 2017; received in revised form 13 September 2018; accepted 16 September 2018

### Abstract:

Based on some findings on the two kinds of Concrete Filled Double Skin steel Tube (CFDST) members with circular or square sections, a new kind of CFDST with octagonal and polygonal section have been investigated under axial and cyclic loading. For this purpose, the outer steel wall has various steel shapes and the inner steel wall is the same as circular section and for some part of analyses, the outer tube is the same as circular section and the inner wall has various steel sections. Primarily, FEM procedure has been verified with some available experimental studies and then, seven composite columns with different section types have been analyzed. The results of analyses exhibited the increase in strength and improvement in hysteresis behavior of the proposed steel sections under cyclic loading.

### Keywords:

Double skin; octagon and polygon section; FE analysis, hysteresis behavior; axial compressive

© 2018 Journal of Urban and Environmental Engineering (JUEE). All rights reserved.

\* Correspondence to: Ebrahim Farajpourbonab, Tel.: +989146145365; Fax: +984137735066  
E-mail: [e.farajpourbonab@gmail.com](mailto:e.farajpourbonab@gmail.com)

## INTRODUCTION

Concrete Filled Double Skin steel Tube (CFDST) columns have been extensively used in the construction of high-rise buildings, arch bridges, and factories in the past years. A number of investigations have been undertaken to study the strength and behavior of these columns under various types of loading. According to Zhang *et al.* (2015), the results of these studies revealed that an increased ductility and strength can be obtained using double skin tubes owing the “composite action” between steel tubes and sandwiched concrete. According to Han *et al.* (2011) and Li *et al.* (2012), this form of column has higher strength as shown in Fig. 1 (uniaxial, flexural, and torsion). The strength to weight ratio is improved significantly by replacement of concrete central part with a hollow steel section. In this case, the confining pressure will be more than CFT column because the inner steel tube would expand outward to increase the confining pressure. The results of experimental studies by Han *et al.* (2004) and Tao *et al.* (2004) on slender CFDST columns and CFDST beam-columns showed that the axial capacity of these columns depend on slenderness ratio such that an increase in slenderness ratio causes a decrease in axial capacity of a CFDST column. Tao *et al.* (2004) reported that in the experiments a greater gain in ductility of the CFDST column and a less local buckling of the inner tube were obtained for sections with smaller  $D_o/t_o$  and  $D_i/t_i$ , correspondingly.

Dong and Ho (2012) used an external steel ring confinement to restrict the dilation of the outer steel tube in CFDST columns. It was found that the external steel rings could considerably prevent the outer steel tube distend, and that significantly improve the uniaxial strength, elastic strength and ductility of CFDST columns when it is compared with those CFDSTs without rings. Junjie *et al.* (2008) found that the strength of the columns with octagonal sections is higher than that of square sections, while it is smaller than that of circular section, and the bearing capacity of samples is related to the ratio of the straight side to the beveled one. Zhaoa *et al.* (2010) showed that CFDST columns significantly improved the behavior of Circular Hollow Section (CHS) in terms of load carrying capacity, failure modes, and energy dissipation. After the cyclic loading, the behavior of samples was affected by the stage of the cyclic loading and the  $D/t$  ratio. Wang, Qian, Liew, and Zhang (2012) indicated that the CFDSTs have a strong resistance under lateral impact loading. Additionally, it was found that outer pipe plays an indispensable role in improving the lateral impact resistance of CFDSTs. The concrete core can absorb a great portion of the impact energy and hence can effectively reduce the local indentation. Concrete core can also assist in preventing the buckling of the tubes. Changing the inner tube thickness hardly affects the lateral impact performance of the CFDST. Recently,

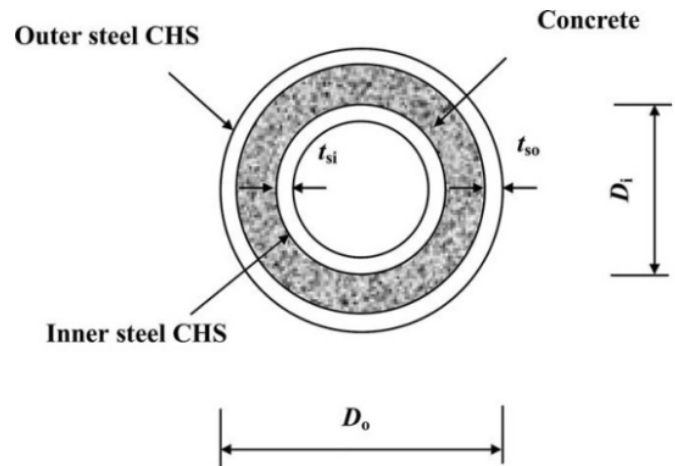


Fig. 1 Details and dimensions of CFDST specimen.

Zhang *et al.* (2015) showed that steel tubes are the key contributors to the blast resistance of CFDST columns. It was found that the influence of concrete strength on the mid-span deflection of the columns is not significant. Whilst the outer tube thickness has a considerable influence on the columns' mid-span deflections, the influence of inner tube thickness is minor. Nirajan & Erremma (2012) had conducted experiments on CFT columns which cross section area of the specimens, was improved through applying the flutes on CFT columns. It was observed that the load resistance of rectangular fluted CFT columns was better than the triangular fluted CFT columns.

According to the past studies, numerical study of the composite columns is required to investigate the parameters that affect the ultimate strength of them and since the effect of cross section shape has a significant role in improving the column's strength. The research on the CFDST columns with octagonal and polygonal sections has not been conducted in previous literature up to now. Therefore, the strength and buckling behavior of CFDST columns with octagonal and polygonal steel shapes have been investigated.

## FINITE ELEMENT MODELING

A finite element modeling has been developed based on the commercial FE package ANSYS 10.0 (2005) to study the behavior of CFDST columns under axial and cyclic loading. Several key issues in the FE modeling are introduced briefly, i.e. the material models for steel and concrete, interface model to simulate the composite action between concrete and steel, element type, mesh, and boundary conditions.

### Characteristics of models

ANSYS R 10.0 (2005) elements and capabilities are as follows. The concrete was modeled using a special concrete element SOLID 65. This element is an 8-node solid brick element that has crushing (compressive) and

cracking (tensile) capabilities. For modeling of steel tube and steel profile, a 3-D solid element SOLID 45 was used. The element has plasticity, swelling, stress stiffening, creep, large strain, and large deflection capabilities. SHELL43 (for the modeling of the rigid plate for load applying) is well suited to model linear, warped, and moderately thick shell structures. The element has plasticity, stress stiffening, creep, large strain, and large deflection capabilities. CONTAC52 (for the modeling of gap between steel and concrete) represents two surfaces that might maintain or break physical contact or might slide relative to each other. The element is capable to support compression members in the normal direction to the surfaces and Coulomb shear friction in the tangential direction.

**Material characteristic**

The stress-strain behavior of in-filled concrete and the steel wall, used for material and geometric static analyses according to Schneider (1998) and Mursi (2003) is given in Figs 2a–c, respectively.

For the concrete element, the elastic modulus ( $E_x=26541.38$ ), the Poisson’s ratio ( $\nu_{xy} = 0.2$ ), the values for the ultimate tensile strength ( $f_t=3.72$ ) and ultimate compressive strength ( $f_c=35$ ) are the properties of isotropic material as shown in Figs 2(a) and 2(b). Considering Fig. 2(c), the behavior of steel is characterized with an initial linear elastic portion of stress-strain relationship with a modulus of elasticity, 209 GPa and up to the yield stress  $f_y$  (ST 37 with  $F_u=370$  N/mm<sup>2</sup>), is equal to 240 MPa, followed by a strain plateau of varying length (strain=0.015) and a following region of strain hardening.

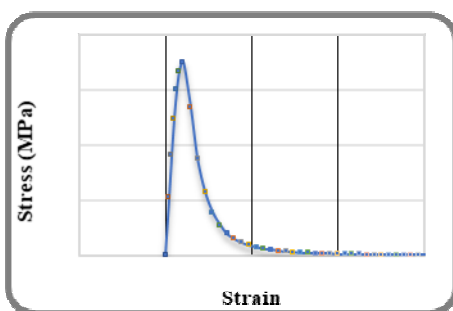


Fig. 2(a) Compressive stress-strain relationship for concrete material.

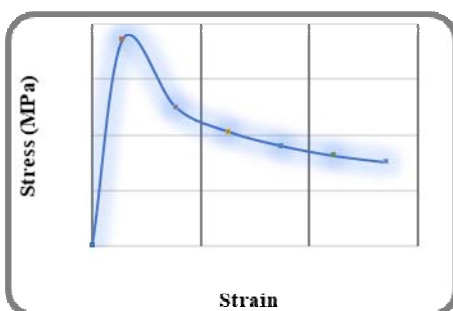


Fig. 2(b) Tensile stress-strain relationship for concrete material.

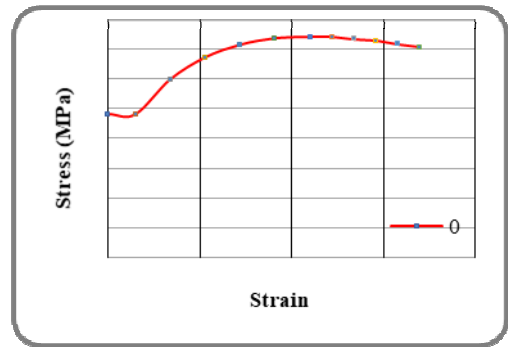


Fig. 2(c) Stress-strain relationship for steel material.

**Verification of finite element modeling**

The accuracy and feasibility of the numerical results was verified by the comparing the calculated results with the experimental observations of Tao *et al.* (2004) under axial loading. Regarding the axial loading, an experimental CFDST column with circular section (sample cc2a) has been used according to the specifications in Table 1.

Figure 3 shows the experimental and numerical axial load - axial deformation response of a CFDST sample under axial loading. It is found that the columns behavior predicted by the finite element analysis closely followed the behavior shown by the experimental results. Consequently, it was observed that the finite element numerical analysis is good enough valid to be implemented in undertaking nonlinear analyses of CFDST columns.

To validate the accuracy of the numerical model for the composite columns under cyclic loading, one previously published test specimen by Guan *et al.* (2003), were used for comparison purpose. The geometrical and material parameters for the test specimen are summarized in Table 2. In this table  $f_{y1}$  and  $f_{y2}$  are yield strengths for the steel tube and the section steel, respectively, and  $f_{cu}$  is cube strength for concrete.

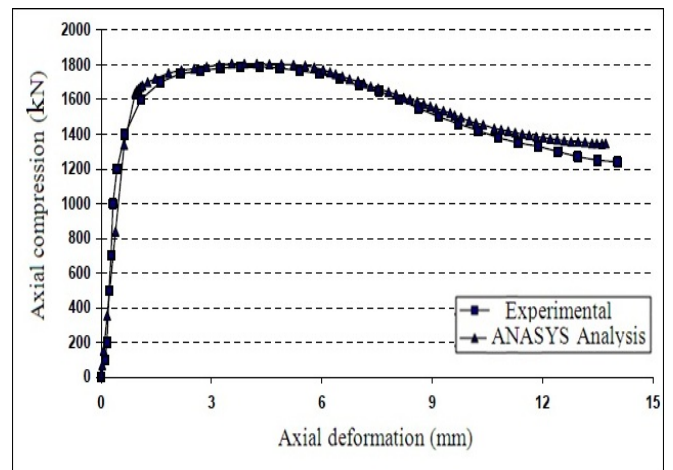


Fig. 3 Experimental and numerical responses of a CFDST column (cc1a Specimen).

**Table 1.** The specifications of the experimental CFDST

Steel Properties			Concrete Properties		$\chi$	L (mm)	$D_i \times t_{si}$	$D_i \times t_{su}$	Specimen
$E_s$ (MPa)	$f_{syi}$ (MPa)	$f_{syo}$ (MPa)	$E_c$ (MPa)	$f'_c$ (MPa)					
200000	396.1	275.9	33300	47.4	0.47	540	48×3	180×3	cc2a

**Table 2.** Geometrical and material properties for the test specimen under cyclic loading

Specimen ID	Section steel			$F_{y2}$ (Mpa)	Steel tube $D \times t$ (mm)	Concrete properties	
	I steel $A_s$ (mm <sup>2</sup> )	$f_{y1}$ (Mpa)	$f_{y1}$ (Mpa)			$F_{cu}$ (Mpa)	n
HC12-1	112	3570	314	269	218*4	74.3	0.5

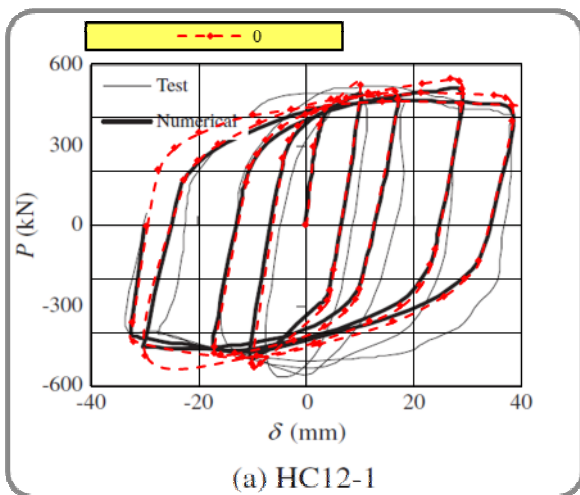


**Fig. 4(a)** Comparison of numerical cyclic load-lateral displacement curve with experimental one.

It should be noted that the cross steel section was made by two "I" steel in the test. **Figure 4a** gives the comparison of computed cyclic load (P) versus lateral deflection ( $\delta$ ) curve with the test one. It can be found that, generally good agreement is obtained between the predicted and tested results. This confirms that the present numerical model can be used with confidence to simulate the behavior of CFT columns under cyclic

loading. **Figure 4b** shows Von Mises stress, equivalent plastic hinge, and yielding areas of verified sample.

**NUMERICAL RESULTS OF SPECIMENS**

**Figures 5–6** show first and second groups of CFDST suggested samples for analyses, respectively. In the first group, the inner tube for all specimens is circular and the outer walls have various steel sections (Po.E12-Cir, Cir-Cir, Oct-Cir, and Sq-Cir). In the second group, the outer tubes for all specimens are circular and the inner walls have variable steel sections (Cir-Po.E12, Cir-Cir, Cir-Po.S12, and Cir-Sq).

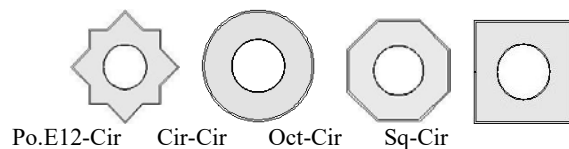


**Fig. 5** Cross section area of first group of CFDST samples.

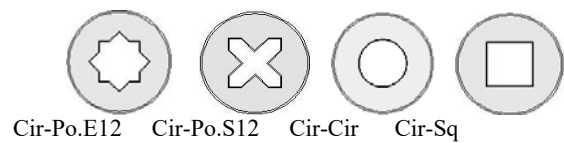


**Fig. 6** Cross section area of second group of CFDST samples.

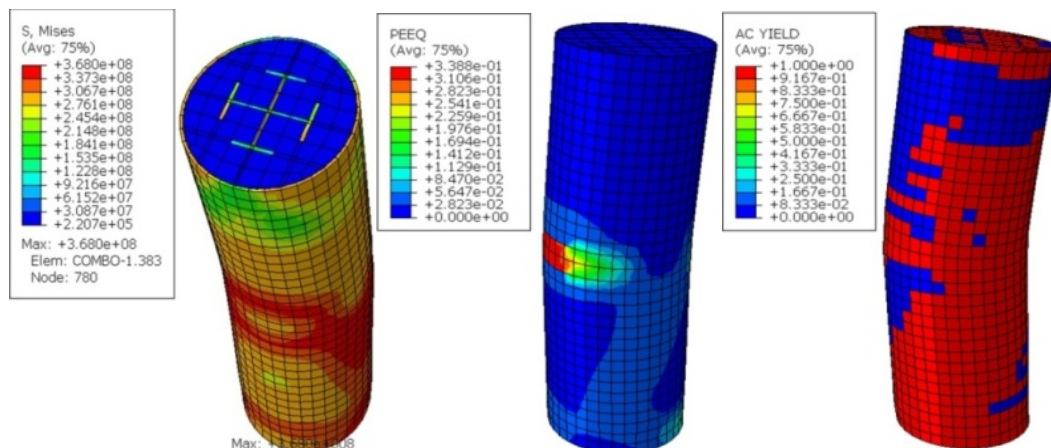


**Fig. 4(b)** (a) Von misses stress, (b) hinge equivalent plastic, and (c) yielding area.

**Table 3.** The specifications of CFDST sam

Sample		Outer tube		Inner tube	
		$D_o \times t_{so}$	Area of outer steel section ( $mm^2$ )	$D_i \times t_{si}$	Area of inner Steel section ( $mm^2$ )
First Group	Po.E12-Cir	725.1×8.12	19163	291.82×4.3	3884
	Cir-Cir	607.96×10.19	19163	291.82×4.3	3884
	Oct-Cir	538.79×9.02	19163	291.82×4.3	3884
	Sq-Cir	591.96×9.87	19163	291.82×4.3	3884
Second Group	Cir-Po.E12	607.96×10.19	19163	346.6×3.47	3884
	Cir-Cir	607.96×10.19	19163	291.82×4.3	3884
	Cir-Po.S12	607.96×10.19	19163	283.6×3.21	3884
	Cir-Sq	607.96×10.19	19163	365.8×3.81	3884

The specifications of CFDST samples are given in Tables 3. The columns are considered as fixed-end columns. For steel:  $f_y = 280$  MPa,  $E_s = 200,000$  MPa and for concrete:  $f'_c = 40.0$  MPa,  $E_c = 30,000$  MPa. L (Lengths of Column) = 3000 mm. The total cross-section area of steel is 23,047  $mm^2$  and the cross-section area of concrete is 204,282  $mm^2$ .

It is noticeable that the thickness of steel wall will be selected according to the design provisions presented by ACI and AISE, in such a way that local buckling does not occur in lower loads.

**NUMERICAL RESULTS OF CFDST SAMPLES UNDER AXIAL LOADING**

To investigate the behavior of CFDST samples in each of the two groups subjected to axial loading, in each case, two rigid plates, located at the top and bottom of the columns, transfer the load. **Figure 7** shows the axial load–axial displacement responses of the circular, octagonal, and square CFDST columns in the first group under axial loading. It indicates that the bearing capacity of the columns with octagonal section when the cross section shape of the outer tubes is variable and the inner tubes have fixed shape, is larger than that with square section, while it is smaller than that with circular section.

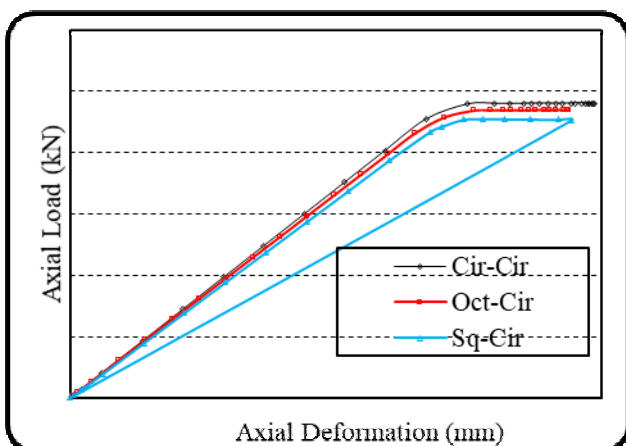


**Fig. 7** Axial load–axial displacement responses of the CFDST columns of group No.1.

**Figure 8** shows the axial load–axial displacement responses of the CFDST columns of second group. It shows that the yield load and stiffness of the polygonal extrados sections (Cir-Po.E12), when the cross section shape of outer tubes is fixed and the inner tubes have variable shapes, are higher than the polygonal soffit and circular CFDST samples. These results clearly show that in polygonal sections, the contact stress between steel and concrete causes higher axial load strength and lesser degradation of strength at larger axial displacement. Therefore, under axial loading, the effect of steel walls on the increase of concrete strength is considerable for the polygonal sections and the steel wall won't be buckled before reaching the steel wall to the yield stress. Thus, the confinement effect of concrete has been increased.

**NUMERICAL RESULTS OF CFDST SAMPLES UNDER LATERAL CYCLIC LOADING**

To investigate the effect of steel section shapes on the hysteretic behavior of CFDST columns, first, a monotonic axial load equal to  $0.3 \cdot f'_c \cdot A_g$  was applied on the top nodes of the column. Then, displacement history according to Hajjar *et al.* (1997) was applied to model the condition of cyclic loading as shown in **Fig. 9**. **Figure 10** is schematically showing boundary condition of specimens and the manner of applying the lateral cyclic loading.

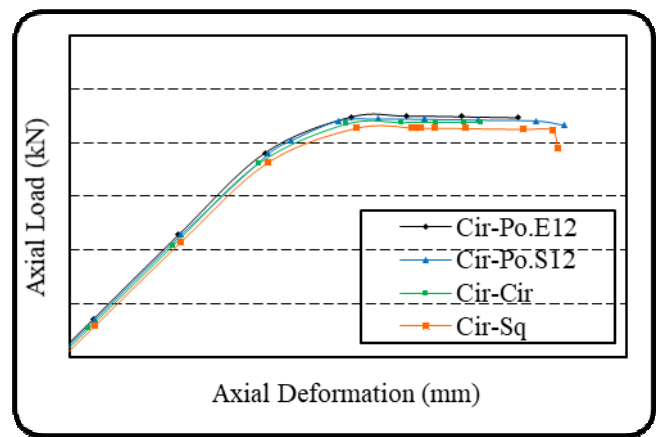


**Fig. 8** Axial load–axial displacement responses of the CFDST columns of group No.2.

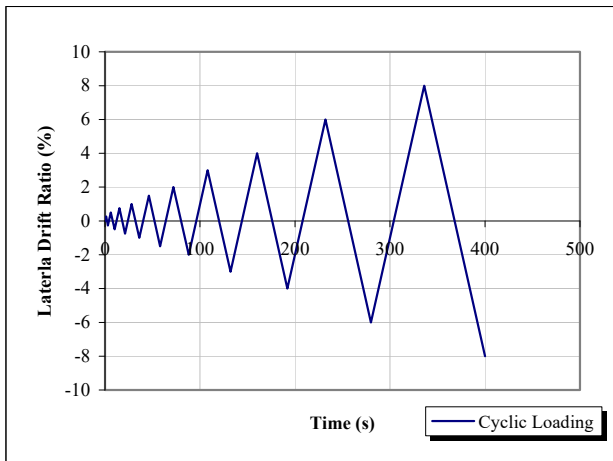


Fig. 9 History of hysteretic loading.

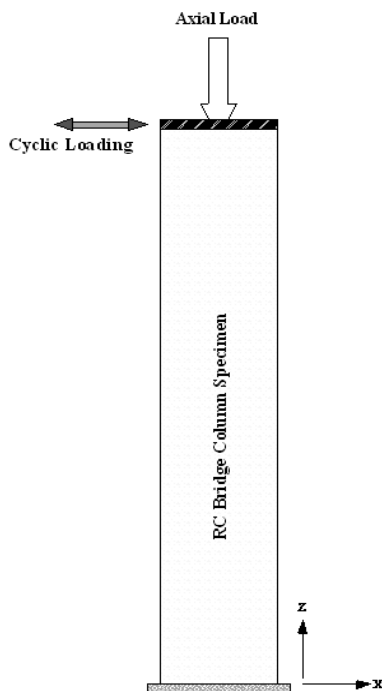


Fig. 10 Boundary condition.

**Hysteretic behavior of CFDST columns**

To investigate the effect of steel section shapes on the hysteretic behavior of CFDST columns, hysteretic responses of first and second groups CFDST samples are shown in Figs 11-12, respectively. The degradation of strength in all selected specimens was begun suddenly at 4% of lateral displacement and that is almost the same for all selected specimens.

**Comparison of hysteresis loops of CFDST columns**

To compare the hysteresis loops of CFDST columns and to investigate the effect of stiffening steel shape on the strength of columns, envelope curves of hysteresis loops for each one of the four samples of group 1 has been illustrated in Fig. 13. Each point in this envelope is the maximum shear force carried by the column in each corresponding cycle of loading.

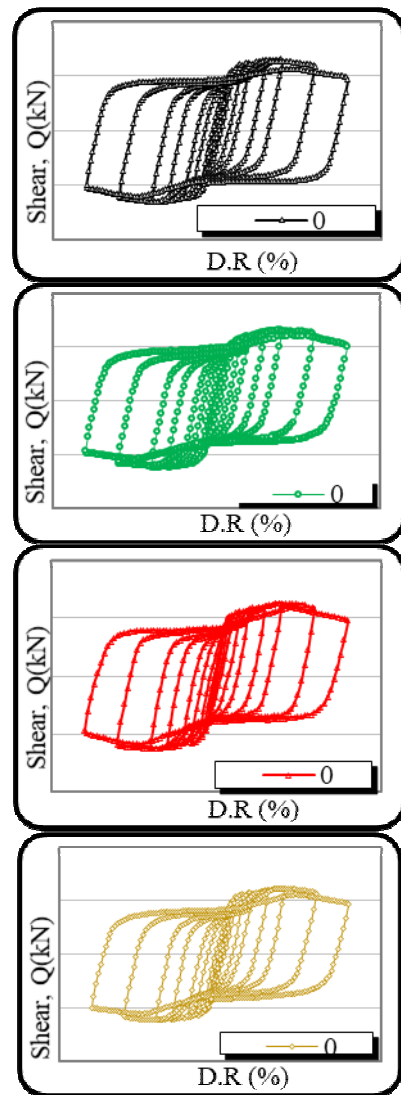


Fig. 11 Hysteretic responses of first group of CFDST samples.

Figure 13 clearly indicates the higher shear strength of polygonal sections (Po.E12-Cir) in comparison with traditional CFDST sections. In addition, it is indicated that the maximum shear strength of the columns with octagonal section is larger than square section and that is smaller than circular section. By considering the samples, it's observed that polygonal, circular, octagonal, and square sections (which both have the same cross section area) have the higher moment of inertia, respectively. In addition, it shows that polygonal, circular, octagonal, and square sections have the higher amount of shear strength, respectively. Therefore, it's concluded that that shear strength capacity of CFDST columns has a positive correlation with the moment of inertia of steel section under cyclic loading.

Figure 14 shows the hysteresis loops of second groups of CFDST columns (when the cross section shapes of outer tubes are fixed and the inner one is variable). This Fig. clearly indicates the lesser degradation of load and higher shear strength of polygonal extrados sections (Cir-Po.E12) in comparison with traditional CFDST sections. In addition, it is

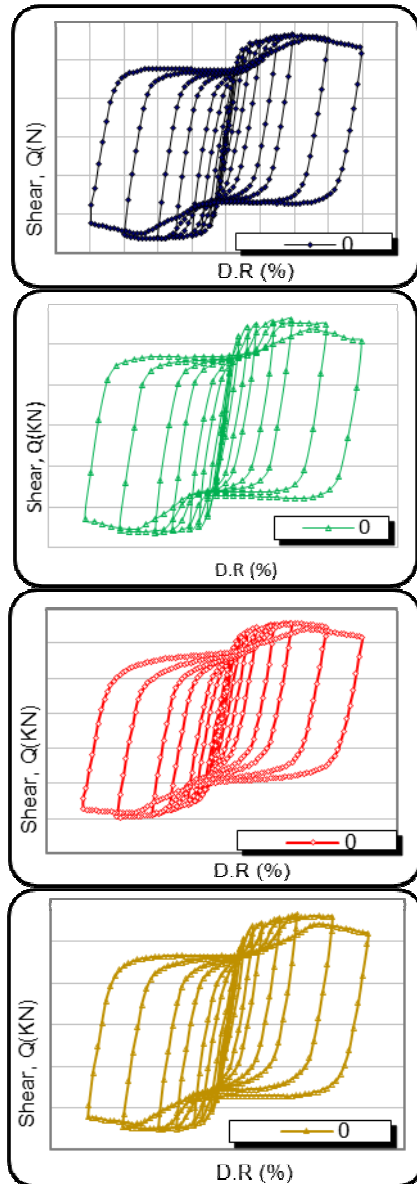


Fig. 12 Hysteretic responses of second group of CFDST samples.

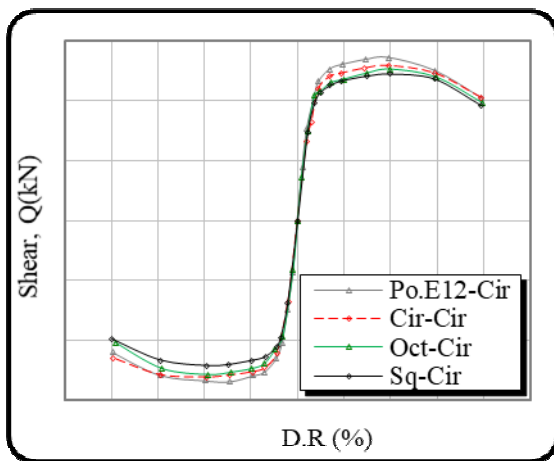


Fig. 13 Lateral load-displacement envelopes between various specimens (First group).

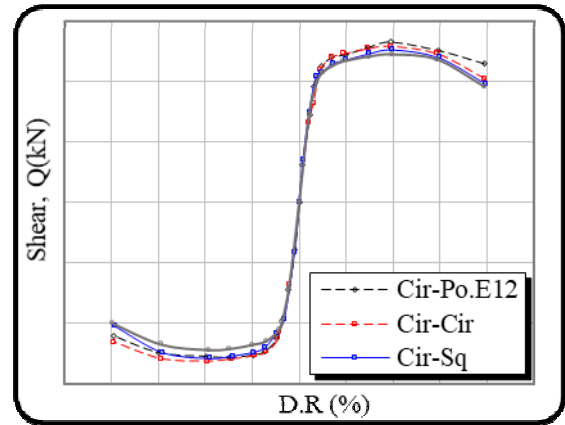


Fig. 14 Lateral load-displacement envelopes between various specimens (Second groups).

indicated that for the second group of CFDST samples, the maximum shear strength of the columns with polygonal soffit section is smaller than other types of CFDST sections.

**Energy dissipation of CFDST samples**

Figures 15–16 illustrate the energy dissipation chart of the first and second groups of CFDST columns in each cycle of loading, respectively. Figures 15–16 clearly show that the amount of energy absorption capacity in polygonal extrados sections (Cir.Po.E12 and Po.E12-Cir) in both each groups is higher than that of traditional CFDST sections. The polygonal extrados sections in both each groups have the best performance regarding stiffness, ductility, and energy absorption capacity. In addition, the energy absorption capacity of the columns with octagonal section is larger than that of square section and that is smaller than circular section. Considering Fig. 16, it is illustrated that for the second group of CFDST samples, the energy absorption capacity of polygonal soffit section is smaller than other types of CFDST sections

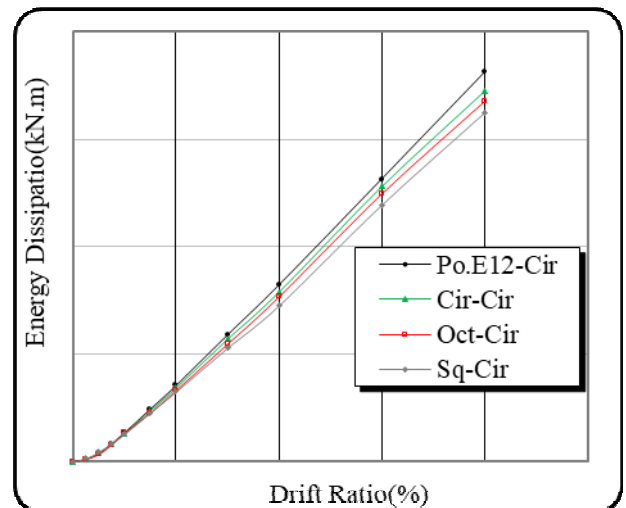
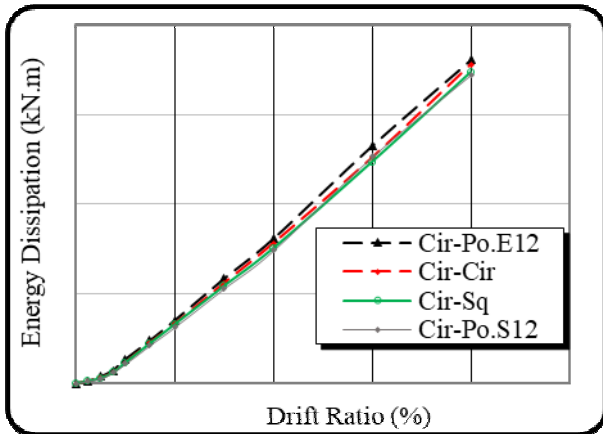


Fig. 15 Energy dissipated- drift ratio diagrams of CFDST Columns (First group).

**Table 4.** Comparison of important parameters of first group of CFDST column

Specimen	Maximum Shear Strength (kN)	Ratio	Energy dissipated (kN.m)	Ratio	Stiffness plastic (N/mm)	Ratio
Sq-Cir	1224	1.00	1625.5	1.00	403.5	1.00
Oct-Cir	1264	1.03	1677	1.03	418.83	1.03
Cir-Cir	1292	1.05	1725	1.06	435.33	1.07
Po.E12-Cir	1358	1.11	1811	1.11	464.17	1.15

**Fig. 16** Energy dissipated- drift ratio diagrams of CFDST Columns (Second groups).

The quantitative comparison between some parameters such as the maximum shear strength, energy dissipated, and the plastic stiffness in cycle No. 10 for the first group of CFDST columns are given in Table 4. For comparison purpose, square section (Sq-Cir) has been selected as a benchmark specimen. Considering the maximum shear strength parameter, polygonal extrados section (Po.E12-Cir) has differences about 11 % more than that of the square section (Sq-Cir). Considering the energy dissipation parameter, polygonal sections have at least a value of 11% improvement in comparison with square CFDST columns. Regarding plastic stiffness parameter, polygonal extrados section exhibited a minimum value of 15% increase against the square section.

It is evident from the results given in Table 4 that new suggested CFDST sections have higher shear strength, better energy absorption capacity, and more appropriate ductility characteristics than that of traditional CFDST columns.

## CONCLUSIONS

This paper reports a finite element analysis of the axial and cyclic behavior of CFDST members with octagonal and polygonal section. The buckling behavior of CFDST specimens with different cross-sectional shapes are compared with those of conventional concrete filled steel tubular members. Following are the conclusions:

1. Confining effect of steel walls on the concrete core and the geometric shape of steel sections were

found the most significant parameters affecting the compressive strength of CFDST columns.

2. Under axial loading when the cross section shape of outer tube is variable and the inner tube is fixed shape, the bearing capacity of the columns with octagonal section is larger than that of square section and smaller than the circular section (group 1).
3. Under axial loading when the cross section shape of the inner tube is variable and the outer tube is fixed, the compressive strength of the polygonal extrados section is higher than polygonal soffit and circular CFDST section (group 2).
4. Considering the results, polygonal, circular, octagonal, and square sections have the higher amount of moment of inertia, shear strength, and energy absorption capacity, respectively. Therefore, the moment of inertia in the steel section was found to be the most significant parameter on the hysteresis behavior of CFDST columns.

## REFERENCES

- ACI 318 (1995) *Building code requirements for reinforced concrete*. American Concrete Institute, Detroit, Michigan.
- AISC/LRFD (2003) *Manual of steel construction, Load and Resistance Factor Design*. American Institute of Steel Construction, Part 4, Composite Columns.
- ANSYS R 10.0 (2005) *Academic*. Structural analysis Guide.
- Dong, C.X., Ho, J.C.M. (2012) Concrete-filled Double-skin Tubular Columns with External Steel Rings. *Proc. Australian Earthquake Engineering Society 2012, Dec 7-9th, Gold Coast, Qld.*
- Guan, P., Wang, Q.X., Zhao, D. Z. (2003) Experimental study on ductility of circular steel tubular columns filled with steel-reinforced concrete. *Earthq. Eng. Eng. Vib.*, **23**(1): 84–9.
- Hajjar, J.F., Goerley, B.C. (1997) A cyclic nonlinear model for concrete filled tubes- formulation. *J. Struct. Engin.*, **123**(6): 736–744.
- Han, L. H., Li, Y. J., Liao, F. Y. (2011) Concrete Filled Double Skin steel Tubular (CFDST) columns subjected to long-term sustained loading. *Thin-walled Struct.*, **49**, 1534-1543.
- Han, L. H., Tao, Z., Huang, H., Zhao, X. L. (2004) Concrete-filled double skin (SHS outer and CHS inner) steel tubular beam-columns. *Thin-walled Struct.*, **42**(9), 1329-1355.
- Junjie, Y., Hanyong, X.U. (2008) Guojun, P., Behavior of concrete-filled double skin steel tubular columns with octagon section under axial compression. *Front. Arch. Civil Engin. China*, **2**(3): 205–210.
- Li, W., Ren, Q. X., Han, L. H. (2012) Behavior of tapered concrete-filled double skin steel tubular stub columns. *Thin-walled Struct.*, **57**, 37-48.

- Mursi, M., Uy, B. (2003) Strength of concrete filled steel box columns incorporating interaction buckling. *J. Struct. Engin.*, **129**(5), 626-639.
- Niranjan, B. R., Erremma, H. (2012) Experimental investigation on reinforced concrete filled steel rectangular fluted columns. *Int. J. Scient. Engin. Res.*, **3**(11), 645-654.
- Schneider S. P. (1998) Axially loaded concrete filled steel tubes. *ASCE J. Struct. Engin.*, **124**(10), 1125-1138.
- Tao, Z., Han, L. H., Zhao, X. L. (2004) Behavior of concrete filled double skin (CHS inner and CHS outer) steel tubular stub columns and beam-columns. *J. Constr. Steel Res.*, **60**, 1129-1158.
- Wang, Y., Qian, X., Liew, J., & Zhang, M. (2012) Concrete-filled pipe-in-pipe composite structure under transverse impact loading. *Proc. 10th ASCCS conference*, Research Publishing Services, Singapore.
- Zhang, F., Wu, C., Wang, H., & Zhou, Y. (2015) Numerical simulation of concrete filled steel tube columns against BLAST loads. *Thin-walled Struct.*, **92**, 82-92.
- Zhang, F., Wu, C., Zhao, X., Li, Z., Heidarpour, A., Wang, H., (2015) Numerical modeling of concrete-filled double-skin steel square tubular columns under blast loading. *J. Perform. Constr. Facil.*, **29**(5), 1 - 12.
- Zhao, X.L., Tong, L., Wei, W.X.Y. (2010) CFDST stub columns subjected to large deformation axial loading. *Engin. Struct.*, **32** (3): 692-703.